Thermochimica Acta 493 (2009) 68–75

Contents lists available at ScienceDirect

Thermochimica Acta

journal homepage: www.elsevier.com/locate/tca

Kinetics study of cold-crystallization of poly(ethylene terephthalate) nanocomposites with multi-walled carbon nanotubes

G. Antoniadis [a], K.M. Paraskevopoulos [a], D. Bikiaris [b], K. Chrissafis [a,*]

[a] Department of Physics, Aristotle University of Thessaloniki, 54124 Thessaloniki, Greece
[b] Department of Chemistry, Aristotle University of Thessaloniki, 54124 Thessaloniki, Greece

ARTICLE INFO

Article history:
Received 2 February 2009
Received in revised form 2 April 2009
Accepted 9 April 2009
Available online 18 April 2009

Keywords:
Poly(ethylene terephthalate)
Multi-walled carbon nanotubes
Nanocomposites
Cold-crystallization
Activation energy

ABSTRACT

A series of PET/MWCNTs nanocomposites were prepared by in situ polymerization using different amounts of multi-walled carbon nanotubes (MWCNTs). The polymerization of poly(ethylene terephthalate) (PET) was prepared by the two-stage melt polycondensation method. The values of the activation energy of the nanocomposites, as calculated with the Kissinger's and Ozawa–Flynn–Wall (OFW) methods, are larger than the ones of pristine PET. These values are 107.9 kJ/mol for PET-0% MWCNTs and 154.0 kJ/mol for PET-1% MWCNTs which is the larger value among all. Avrami plots present a linear portion, almost parallel to each other, which is followed by a deviation at larger temperatures. Straight lines are obtained from Ozawa plots only for PET-0.25% MWCNTs at least for three different heating rates. The dependence of the activation energy on the degree of conversion, from the Avrami, Malek and Ozawa plots, gives indications that for the kinetic description of the cold-crystallization of PET/MWCNTs cannot be used only one crystallization mechanism which obeys to Avrami equation. Only for the PET-0.25 one crystallization mechanism can be used at least for the major part of the crystallization conversion. So, in order to describe their crystallization mechanisms at least two mechanisms with different activation energies must be used. These two mechanisms maybe are taking part in different degree of crystallization conversions for every nanocomposite.

1. Introduction

Poly(ethylene terephthalate) (PET) is of major industrial importance due to its low cost and high performance (since it has high glass transition and melting temperatures) as well as good physical properties. It has been found a variety of applications such as in textile fibers, films, bottle containers, food packaging materials, engineering plastics in automobiles, electronics, etc. Its properties depend mainly on the degree of orientation of the polymer chains and the degree of crystallinity.

PET-nanotube composites have been studied recently for their possible application in fuel cells [1,2] flexible vapour sensors [3], conductive fibers [4] and composite materials with functionalized [5] and acid-treated [6] nanotubes.

The crystallization behaviour of polymer composites and their crystallization kinetics as a function of processing conditions are of great importance particularly for the analysis and design of processing operations. Therefore, the crystallization behaviour and structural development of MWCNT-reinforced polymer nanocomposites should be analyzed to realize the full potential of MWCNTs for application in thermoplastic matrix-based polymer nanocomposites. Previous studies of single-walled carbon nanotubes (SWNTs) and multi-walled carbon nanotubes (MWNTs) dispersed in polypropylene [7–9], SWNTs in poly(vinyl alcohol) [10,11] and MWNTs in nylon-6 [12,13] suggested that nanotubes can act as nucleating agents. These observations are similar to those for layered silicate [14,15] and polyhedral oligomeric silsesquioxanes (POSS)-based semicrystalline polymer nanocomposites [16,17] where the increased interfacial area alters the kinetics and energetics of nucleation and growth, the overall crystallite fraction, the morphological organization and even the unit cell structure, and results in dramatic changes in the mechanical properties of the nanocomposites [18]. The incorporation of MWCNTs decreases the cold-crystallization peak temperature as different authors have shown [5,19–21].

However, as far as we know, there are no reports about the kinetics of non-isothermal cold-crystallization behaviour of (PET/MWCNTs) nanocomposites, and for this reason we have studied in detail the crystallization kinetics of mentioned nanocomposites, using differential scanning calorimetry (DSC).

* Corresponding author. Tel.: +30 2310 998188; fax: +30 2310 998188.
E-mail address: hrisafis@physics.auth.gr (K. Chrissafis).

0040-6031/$ – see front matter © 2009 Elsevier B.V. All rights reserved.
doi:10.1016/j.tca.2009.04.005

2. Experimental

2.1. Materials

Dimethyl terephthalate (DMT) (99%), ethylene glycol (EG) (99%), zinc acetate [$Zn(OCOCH_3)_2{\cdot}2H_2O$] and antimony trioxide (Sb_2O_3) used for synthesis of PET were purchased from Aldrich Chemical Co. Polyphosphoric acid (PPA) used as heat stabilizer was supplied from Fluka. The MWCNTs used in this work were synthesized by chemical vapour deposition (CVD) and were supplied by Nanothinx (Patra, Greece). They had a diameter between 9 and 20 nm and a length >5 μm. All other materials and solvents used for the analytical methods were of analytical grade.

2.2. PET synthesis and preparation of PET/MWCNTs nanocomposites

For the synthesis of PET, the reaction mixture comprised 31 g (0.50 mol) of EG, and 44.134 g (0.227 mol) of DMT ester (molar ratio of EG/DMT = 2.2), 50 ppm of $Zn(OCOCH_3)_2{\cdot}2H_2O$ as transesterification catalyst and 950 ppm of Sb_2O_3 as polycondensation catalyst.

The reaction mixture, in the transesterification step was heated to the final temperature (270 °C) under argon atmosphere with the stirring at a constant speed (500 rev/min). The reaction was completed after ≈3 h, when almost all the theoretical amount of methanol (18.4 ml) had been collected. In the second step (polycondensation) the catalyst Sb_2O_3 was added and a vacuum (4.0 Pa) was applied slowly (over about 30 min), to avoid excessive foaming and to minimize oligomer sublimation that is a potential problem during melt polycondensation. The temperature remained stable at 270 °C while stirring speed was increased to 720 rev/min. Polycondensation continued for about 1.5 h until the agitator speed decreased to 50–60 rev/min, due to the increasing viscosity of the melt. When the polycondensation reaction was completed, the reaction tube was broken to get the product out of the tube. All polyester samples, after the glass particles were removed with a grinder, were grounded in a mill, sieved, washed with methanol and dried at 110 °C for 12 h.

For the preparation of PET/MWCNTs the same procedure was applied with the only difference that MWCNTs were added from the beginning of transesterification reaction. The prepared nanocomposites were containing 0.25, 0.5, 1 and 2 wt% MWCNTs and are named as PET-0.25, PET-0.5, PET-1 and PET-2, respectively, while the neat polyester was named as PET-0.

2.3. Measurements

Intrinsic viscosity [η] measurements on the isolated polymers were performed using an Ubbelohde viscometer cap. Ic at 25 °C in phenol/tetrachloroethane 60/40 w/w at a solution concentration of 1 wt%.

The differential scanning calorimetric (DSC) measurements were carried out in a Setaram DSC-141 calorimeter. Temperature and energy calibrations of the instrument were performed, for different heating rates, using the well-known melting temperatures and melting enthalpies of high-purity Zinc (Zn), Tin (Sn) and Indium (In) supplied with the instrument. Bulk-shaped specimens weighing about 6 mg were crimped in aluminium crucibles; an empty aluminium crucible was used as reference. A constant flow of nitrogen was maintained to provide a constant thermal blanket within the DSC cell, thus eliminating thermal gradients and ensuring the validity of the applied calibration standard from sample to sample. The samples were first melted to 280 °C, they remained for 5 min and then, they rapidly cooled (quenching). After this, the samples were heated till 280 °C with different heating rates (2.5, 5, 10, and 15 °C/min). From these scans, the glass transition (T_g), the cold-crystallization temperature (T_{cc}), the melting temperature (T_m) and the heat of fusion (ΔH) of the samples were measured.

3. Theoretical background

Kinetic analysis of solid-state transformations is usually based on a single-step kinetic equation:

$$\frac{da}{dt} = k(T)f(\alpha) \tag{1}$$

where $k(T)$ is the rate constant, t is the time, T is the temperature, α is the extent of conversion from the amorphous (liquid or solid) to crystalline phase, and $f(\alpha)$ is the reaction model related to the mechanism. The explicit temperature dependence of the rate constant is introduced by replacing $k(T)$ with the Arrhenius equation, which gives:

$$\frac{d\alpha}{dt} = A\exp\left(\frac{-E}{RT}\right)f(\alpha) \tag{2}$$

where A (the preexponential factor), E (the activation energy) are the Arrhenius parameters and R is the gas constant. For non-isothermal conditions, $d\alpha/dt$ in Eq. (2) is replaced with $\beta\,(d\alpha/dT)$, where β (=dT/dt), is the heating rate [22]. The ratio of the kinetic process $d\alpha/dt$ is proportional to the measured specific heat flow φ, normalized per sample mass (W/g):

$$\frac{d\alpha}{dt} = \frac{\varphi}{\Delta H_c} \tag{3}$$

where ΔH_c corresponds to the total enthalpy change associated with the crystallization process. The extent of conversion α can be easily obtained by partial integration of non-isothermal thermal analysis curve.

The crystallization kinetics is usually interpreted in terms of the standard nucleation-growth model formulated by Johnson–Mehl–Avrami (JMA) [23,24]. This model describes the time dependence of the extent of conversion α, usually written in the following form:

$$\alpha = 1 - \exp[-(kt)^n] \tag{4}$$

where k is the Avrami crystallization rate constant, which is a function of temperature and in general depends on both the nucleation frequency and the crystal growth rate, and the Avrami kinetic exponent n is a parameter which reflects the nucleation frequency and/or the growth morphology. It should be noted that both k and n are constants specific to a given crystalline morphology and type of nucleation for a particular crystallization condition [25] and that, based on the original assumptions of the theory, the value of the Avrami exponent n should be an integer ranging from 1 to 4.

It should be mentioned that in non-isothermal crystallization, the k and n parameters do not have the same physical meaning as in the isothermal crystallization because the temperature changes instantly in the non-isothermal crystallization [19]. In this case, k and n are two adjustable parameters to be fitted to the data. However, the use of Eq. (4) can still provide further insight into the kinetics of non-isothermal crystallization.

The Avrami rate equation can be obtained from Eq. (4) by differentiation with respect to time:

$$\frac{d\alpha}{dt} = kn(1-\alpha)[-\ln(1-\alpha)]^{1-1/n} \tag{5}$$

Eq. (5) is usually referred to as the JMA equation, and it is frequently used for the formal description of thermal crystallization data. It should be emphasized, however, that the validity of the JMA equation is based on the following assumptions: (a) isothermal crystallization conditions, (b) low anisotropy of growing crystals, (c) homogeneous nucleation or heterogeneous nucleation at randomly

Table 1
Glass transition (T_g), cold-crystallization (T_{cc}) and melting temperatures (T_m) of the PET nanocomposites after quenching and heating with 10 °C/min.

Material	MWCNTs (wt%)	[η] (dl/g)	Insoluble content (%) [36]	T_g (°C)	T_{cc} (°C)	T_m (°C)	ΔH_m (J/g)
PET-0	0	0.57	–	76.4	134.5	250.3	32.2
PET-0.25	0.25	0.63	–	78.6	130.0	250.5	27.0
PET-0.5	0.5	0.52	–	77.7	127.6	249.6	25.2
PET-1	1	0.49	–	76.0	127.3	245.6	26.8
PET-2	2	0.31	2.5	64.8	119.4	226.4	31.6

dispersed second-phase particles, and (d) growth rate of new phase controlled by temperature and independent of time.

Henderson [26,27] has shown that the validity of the JMA equation can be extended in non-isothermal conditions if the entire nucleation process takes place during the early stages of the transformation and it becomes negligible afterward. The crystallization rate is controlled only by temperature and does not depend on the previous thermal history. Although the limits of applicability of the JMA equation are well known, in practice it is not so easy to verify whether or not the conditions of applicability are fulfilled. Several methods have been proposed to test the applicability of the JMA model and we examined our non-isothermal data by two of them.

The most popular testing method for non-isothermal data is an inspection of the linearity of the Avrami (JMA) plot. Matusita et al. [28], extending the use of the JMA equation, have suggested an equation, which is applicable for non-isothermal crystallization and is given by:

$$\ln[-\ln(1-\alpha)] = -n\ln(\beta) - 1.052m\frac{E_c}{RT} + \text{const.} \quad (6)$$

where α is the volume of the fraction crystallized (the extent of conversion) at any temperature and m, n are numerical factors depending on the nucleation process and growth morphology, respectively. Here, n is equal to $(m+1)$ for a quenched glass containing no nuclei and n is equal to m for a glass containing a sufficiently large number of nuclei. Also, $m=3$ for three-dimensional growth of crystal particles, $m=2$ for two-dimensional growth, and $m=1$ for one-dimensional growth. The plot of $\ln[-\ln(1-\alpha)]$ as a function of reciprocal temperature $1/T$ should be linear. Nevertheless, it is well known that a double logarithmic function, in general, is not very sensitive to subtle changes to its argument. Therefore, one can expect to observe substantial linearity in the plots of $\ln[-\ln(1-\alpha)]$ versus $1/T$ even in the case that the JMA model is not fulfilled.

Another test for the applicability of the JMA model is based on the properties of the $y(\alpha)$ and $z(\alpha)$ functions (see below). Taking into account Eqs. (1)–(3), the kinetic equation for the JMA model can be written as:

$$\varphi = \Delta H_c A \exp\left(\frac{-E}{RT}\right) f(\alpha) \quad (7)$$

where the function $f(\alpha)$ is an algebraic expression of the JMA model:

$$f(\alpha) = n(1-\alpha)[-\ln(1-\alpha)]^{1-1/n} \quad (8)$$

The $f(\alpha)$ function should be invariant with respect to procedure parameters such as sample mass and heating rate for non-isothermal conditions. Malek has shown [29–31] that the functions $\varphi(t)$ and $\varphi(T)$ are proportional to the $y(\alpha)$ and $z(\alpha)$ functions that can easily be obtained by a simple transformation of DSC data. In non-isothermal conditions these functions are defined as follows:

$$y(\alpha) = \varphi \exp\left(\frac{E_c}{RT}\right) \quad (9)$$

$$z(\alpha) = \varphi T^2 \quad (10)$$

For practical reasons the $y(\alpha)$ and $z(\alpha)$ functions are normalized within the 0–1 range. The maxima exhibited by the $y(\alpha)$ and $z(\alpha)$ functions are defined as α_M and a_p^∞, respectively. The maximum of the $z(\alpha)$ function a_p^∞ is a constant for the JMA model ($a_p^\infty = 0.632$) and a characteristic "fingerprint" for it [30,32].

4. Results and discussion

4.1. Characterization of nanocomposites

The addition of MWCNTs has a great influence to the molecular weight of the produced nanocomposites. As can be seen from Table 1 the intrinsic viscosity ([η]) increases at low MWCNTs content and gradually decreases by increasing the content. Thus the lowest intrinsic viscosity was calculated at the sample containing 2 wt% MWCNTs. This is because MWCNTs due to their surface hydroxyl and carboxyl groups can act as multifunctional additives. In similar nanocomposites containing SiO_2, which can act also as multifunctional additives, in low amounts can act as chain extender increasing the MW of the polymer while in higher contents due to the extended reactions branched and crosslinked macromolecules are formed reducing the MW [33,34]. It is known that the hydrodynamics dimensions of branched polymers in solution are smaller than those of linear polymers with the same molecular weight [35]. The intrinsic viscosity analysis calculates the molecular weight of polymers based on hydrodynamic size in solution. Therefore, in the case that branched and crosslinked polymers are in a sample, as in case with higher MWCNTs, lower molecular weights will be calculated from the real one. This may explain the gradual decrease that observed in molecular weight of the PET samples with concentrations of MWCNTs nanotubes greater than 0.25 wt%. The sample due to these extended crosslinked macromolecules has an insoluble content 2.5 wt%.

Fig. 1 shows the DSC thermograms for all the studied materials heated with rate of 10 K/min, after quenching the initially prepared samples. In these plots the glass transition, the cold-crystallization and the melting peaks are presented. These samples have a single

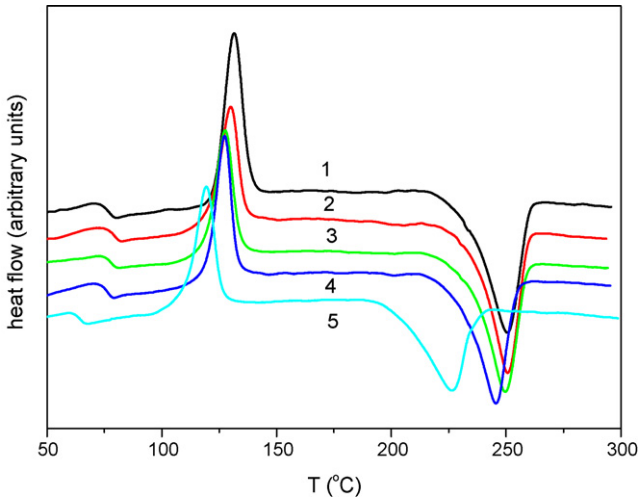

Fig. 1. Heating after quenching: the glass transition, the cold-crystallization and the melting peaks are presented: (1) PET-0; (2) PET-0.25; (3) PET-0.5; (4) PET-1; (5) PET-2.

melting point while in the first scans all the samples presented a double melting peak with different overlapping percentage [37]. This is usual in polyesters due to the formation of crystals with different perfection [38–45]. The melting temperature shifts to lower values by increasing the MWCNTs content (Fig. 1, Table 1). The slight decrease in the melting point might result from a specific interaction between PET and MWCNTs, and the homogeneous dispersion of MWCNTs affects the formation of PET crystals. The effect of MWCNTs on crystallization mechanism was extensively discussed in our previous study [37] and for this reason in the present study only their effect on cold-crystallization was evaluated.

From Fig. 1 one can see that the glass transition temperature (T_g) and cold-crystallization peak temperature (T_{cc}) are apparently influenced by MWCNTs. Neat PET has a T_g value 76.4 °C and for nanocomposites containing 0.25 and 0.5 wt% MWCNTs the T_g was recorded at higher temperatures 78.6 and 77.7 °C, respectively. It is well known that T_g shows the mobility of molecular chain segments, the lower the T_g, the easier the motion of the chain segments. The results in these PET/MWCNTs nanocomposites are in agreement with those reported in literature: in nanocomposites, in the most cases, it was found that T_g shifts to higher values when some interactions are taking place between polymer and nanoparticles [46]. As mentioned, usually the T_g of a polymeric matrix tends to increase with the addition of carbon nanotubes, due to the interactions between the polymer chains and the nanotubes and to the reduction of macromolecular chain mobility at the zone surrounding the nanotubes [47]. Wang reported [48] that due to polymer-filler interaction the adsorption of the polymer chains on the filler's surface reduces the mobility of the macromolecular segments. This transition zone surrounding the nanotubes exhibits higher modulus and T_g, both of which are gradually reduced with increasing distance from the filler surface. However, in PET/MWCNT nanocomposites containing 1 and 2 wt% the T_g temperatures were recorded at 76 and 64.8 °C, respectively. This behaviour was not expected since the particular samples are branched or partially crosslinked and in such polyesters the T_g slightly shifts to higher values due to the restriction of macromolecular segment movement [49,50]. As can be seen from Table 1 the insoluble content of sample containing 2 wt% MWCNTs is 2.5 wt%, which is an indication that in particular samples crosslinked macromolecules were formed. So it seems that MWCNTs, which have surface –OH and –COOH groups can act as multifunctional additives crating branched macromolecules at low concentrations and crosslinked at higher as in the case of 2 wt% MWCNTs. The above results suggest that the incorporation of higher amounts of MWCNTs in PET matrix is favourable to the motion of PET chain segments and this behaviour should be attributed to the effect of MWCNTs. It seems that MWCNTs acting as multifunctional agents macromolecules with sorter segments can be prepared. This reduction is in good agreement with some research studies in PET nanocomposites, which reported that T_g of PET is reduced due to the incorporation of nanoparticles in polymer matrix [5,19,51]. Such nanoparticles can be SiO_2 and MWCNTs, which have surface reactive groups and are also used in our studies.

For cold-crystallization behaviour, the T_{cc} values of nanocomposites are lower than that of pure PET. For example, T_{cc} is decreased from 134.5 °C of neat PET to 119.4 °C of PET-2. The decrease of T_{cc} means that the cold-crystallization of PET in nanocomposites becomes easier than in neat PET. This can be attributed to the lower molecular weight that the samples with increased MWCNTs content have, and as was found from a previous study in aliphatic polyesters the cold-crystallization temperature increases by increasing the molecular weight of polyester [52]. Furthermore, the lower cold-crystallization temperature can be attributed to MWCNTs which acting as nucleating agents is enhancing the crystallization of PET macromolecules. This is probably due to the fact that MWCNTs have higher surface area in contact with PET matrix and thus induce a heterogeneous nucleation effect [53].

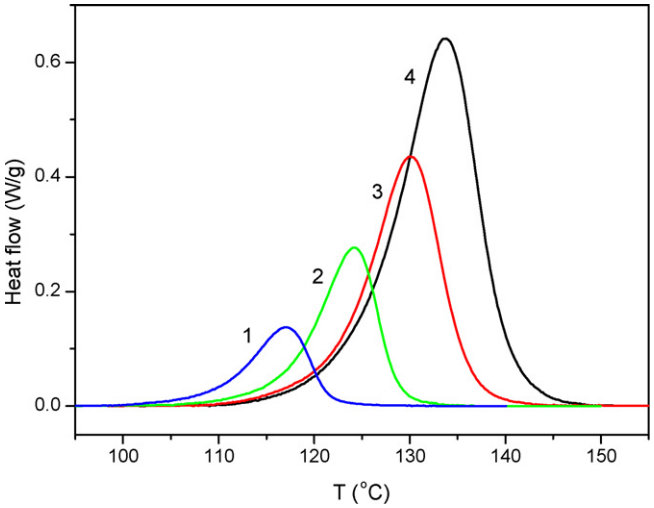

Fig. 2. Cold-crystallization peaks of PET-0.25 with different heating rates: (1) β = 2.5 °C/min; (2) β = 5 °C/min; (3) β = 10 °C/min; (4) β = 15 °C/min.

4.2. Crystallization kinetic study

The study of the crystallization kinetics follows two steps: at the first step the activation energy is calculated independently of the reaction model and at the second step the crystallization mechanism and the appropriate kinetic model is discussed. For the kinetic study non-isothermal measurements with different heating rates are used. In Fig. 2 the exothermic cold-crystallization peaks of PET-0.25 for different heating rates are presented as an example. It is clear that the peak shifts to higher temperatures with increasing heating rate, while at the same time the peak height increases. The area under the crystallization exotherm, in the heat flow versus time diagram (total change of enthalpy during the crystallization), remains almost constant.

This behaviour can be understood if we accept that the crystallization of an amorphous state consists of two individual processes: nucleation and growth. For glasses to nucleate, a certain period of incubation is necessary. As the heating rate increases, the time available for a desired temperature to be reached is reduced and thus crystallization lags and initiates at relatively higher temperatures, i.e., the T_{cc} correspondingly shifts to higher temperature. Generally, glasses undergo structural relaxation through which they transform from a metastable to a stable state during crystallization. The time for this transformation is shortened with increasing heating rate, preventing the entire energy of structure relaxation from being released. This part of unreleased energy is contained in the crystallization enthalpy, which is determined by the area of the DSC exotherm.

4.2.1. Determination of the activation energy

For the determination of the activation energy isoconversional methods is preferable to be used [54]. Two of them, the Kissinger and Ozawa, Flynn and Wall (OFW) methods are used for comparison reasons.

4.2.1.1. Kissinger's method. For the determination of the activation energy of cold-crystallization (E_{cc}) we considered the Kissinger formula [55,56], which is most commonly used in analysis of crystallization data. This formula that holds in very general cases is

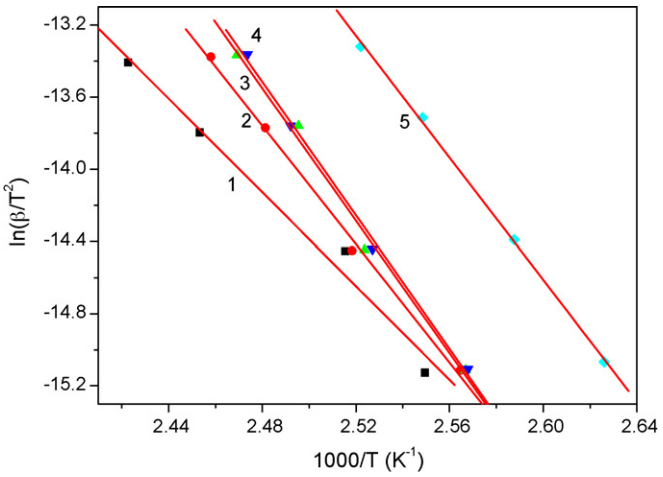

Fig. 3. Kissinger's plots and the corresponding straight regression lines for all the studied materials: (1) β = PET-0; (2) β = PET-0.25; (3) β = PET-0.5; (4) β = PET-1; (5) β = PET-2.

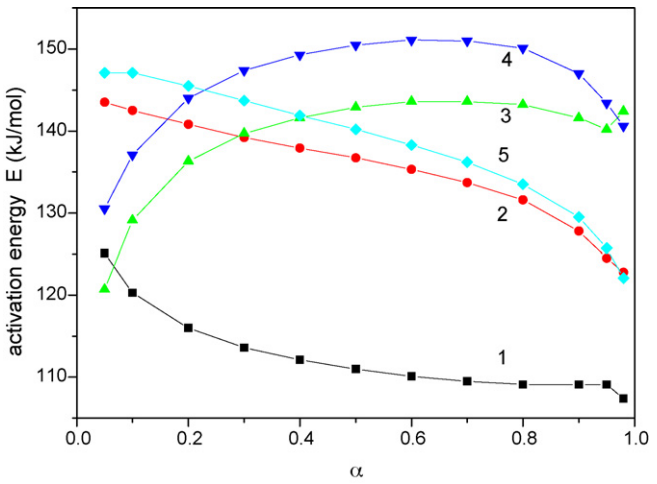

Fig. 4. Effective activation energy as a function of relative extent of crystallization for cold-crystallization of all studied materials obtained using the OFW method: (1) PET-0; (2) PET-0.25; (3) PET-0.5; (4) PET-1; (5) PET-2.

Table 2
The values of E_{cc} as they were calculated by Kissinger's method.

Material	Activation energy E_{cc} (kJ/mol)
PET-0	107.9
PET-0.25	136.6
PET-0.5	152.5
PET-1	154.0
PET-2	140.7

suggested to be valid for crystallization and has the form:

$$\ln\left(\frac{\beta}{T_{cc}^2}\right) = -\frac{E_{cc}}{RT_{cc}} + \text{const.} \quad (11)$$

where R is the universal gas constant, β (=dT/dt) the heating rate and T_{cc} the crystallization's peak temperature. The value of E_{cc} is obtained from the slope of $\ln(\beta/T_{cc}^2)$ versus $1/T_{cc}$ plot. In Fig. 3 these plots and the corresponding straight regression lines for all the studied materials are presented. The calculated E_{cc} values of all the materials (in kJ/mol) are summarized in Table 2. From the values of the activation energy presented in Table 2 it is obvious that as the quantity of MWCNTs is increased the value of the activation energy is increased also, presenting a maximum value for PET-1.

4.2.1.2. OFW method. The isoconversional OFW [57–59] method is the second one, which was used to calculate the activation energy for different extent of conversion values. This is in fact a "model free" method which involves measuring the temperatures corresponding to fixed values of α from experiments at different heating rates β. Plotting $\ln(\beta)$ against $1/T$ according to Eq. (2):

$$\ln(\beta) = \ln\left[\frac{Af(\alpha)}{(\mathrm{d}\alpha/\mathrm{d}t)}\right] - \frac{E_{cc}}{RT} \quad (12)$$

should give straight lines, the slopes of which are directly proportional to the activation energy ($-E_{cc}/R$).

If the determined activation energy is the same for the various values of α_i, the existence of a single-step reaction can be concluded with certainty. In contrast, a change of E_{cc} with increasing degree of conversion is an indication of a complex reaction mechanism that invalidates the separation of variables involved in the OFW analysis [58]. These complications are especially serious if the total reaction involves competitive reaction mechanisms. The plots of activation energy versus α of all of the materials are shown in Fig. 4.

It is clear from these plots that all the values of the activation energy of the nanocomposites are larger than the ones of pristine PET. As can be seen from Fig. 4 there is a continuously increase of activation energy from sample 1 till the sample 4. However, in the sample 5, which has an extended crosslinked content the activation energy is decreased, since these macromolecules reduces the crystallization rate. The activation energy presents a good stability in the region of $0.2 < \alpha < 0.8$ and the maximum value of E in this area corresponds to PET-1. The same trend present the values of the activation energy calculated with Kissinger's method.

Vyazovkin et al. [60] calculated the effective activation energy E for neat PET by the integral isoconversional method. This exhibited a decrease in its value with increasing extent of crystallization conversion from 120 to 50 kJ mol^{-1} (reported for the similar degree of crystallinity range of 0.05–0.95 which was used to obtain the E value for PET in this work). These E values are in a wider range than the values obtained in this work. This may be attributed to the difference in the average molecular weights of the PET used [60] or to the difference in the type and concentration of heterogeneous nuclei presented in the resins [61]. To our knowledge, there are no reports about the activation energy of cold-crystallization for (PET/MWCNTs) nanocomposites.

4.2.2. Study of the crystallization mechanism

As it is mentioned in the preceding Section 3, in order to describe the crystallization process mainly the JMA model is used. To test further this, we examined the applicability of the JMA model to the experimental data by the aforementioned methods, assuming a single-step crystallization process. Figs. 5 and 6 present the Avrami plots of $\ln[-\ln(1-\alpha)]$ versus $1/T$ at different heating rates using Matusita's equation, for PET-0 and PET-0.25, as examples for comparison reasons. Each curve has a linear portion, which is followed by a deviation at larger temperatures. Usually, this deviation is considered to be due to the secondary crystallization, which is caused by the spherulite impingement in the later stage. The linear portions are almost parallel to each other. These correspond to a wide temperature and crystallization conversion range ($0.05 < \alpha < 0.80$). The results are analogous for all the materials and only in neat PET this area is narrower.

Thus, to a first approximation, the experimental data can be studied with the nucleation–growth JMA model according to Eq. (5) for the linear portions. From the slopes of these regression lines we can calculate the mE_{cc} values using Eq. (6). Then, taking into account the value of the activation energy E_{cc} derived from the application of the Kissinger's model (see Table 3) it can be calculate the m factor. The mE_{cc} values as well as the values of kinetic

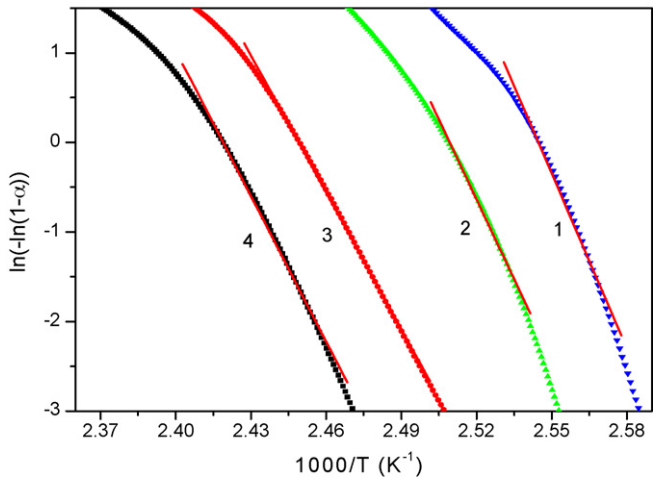

Fig. 5. Plot of $\ln[-\ln(1-\alpha)]$ versus $1/T$ at different heating rates for sample PET-0: (1) $\beta = 2.5\,^{\circ}$C/min; (2) $\beta = 5\,^{\circ}$C/min; (3) $\beta = 10\,^{\circ}$C/min; (4) $\beta = 15\,^{\circ}$C/min.

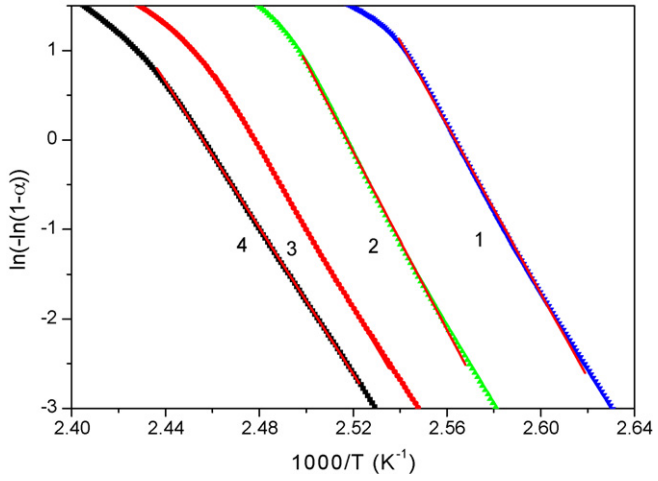

Fig. 6. Plot of $\ln[-\ln(1-\alpha)]$ versus $1/T$ at different heating rates for sample PET-0.25: (1) $\beta = 2.5\,^{\circ}$C/min; (2) $\beta = 5\,^{\circ}$C/min; (3) $\beta = 10\,^{\circ}$C/min; (4) $\beta = 15\,^{\circ}$C/min.

exponent m for each of the experimental heating rates, given in Table 3, were obtained from the plot using least squares fitting. The values of m are decreased due to the addition of MWCNTs into pristine PET. As to our knowledge, there are no reports about the linearity of the Avrami plot for non-isothermal cold-crystallization of (PET/MWCNTs) nanocomposites, or values for the m factor.

Ozawa theory [58,59] has been also used to describe the non-isothermal crystallization kinetics of polymers, which can be described as based on Avrami theory. According this theory the degree of conversion α at a temperature T can be calculated as:

$$1 - a = \exp\left(\frac{-k(T)}{\beta^n}\right) \tag{13}$$

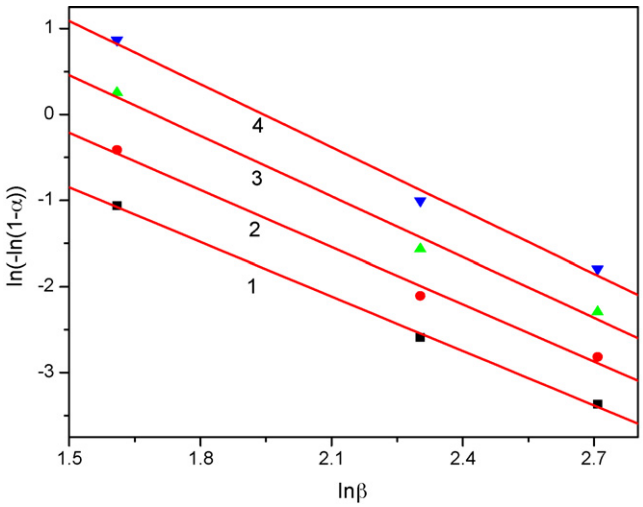

Fig. 7. Ozawa plots for non-isothermal cold-crystallization of PET-0.25 with heating rates 5, 10, 15 °C/min: (1) $T = 121\,^{\circ}$C; (2) $T = 123\,^{\circ}$C; (3) $T = 125\,^{\circ}$C; (4) $T = 127\,^{\circ}$C.

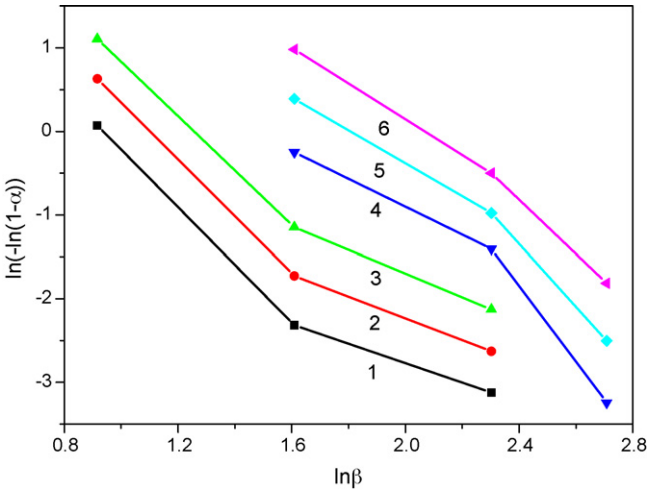

Fig. 8. Ozawa plots for non-isothermal cold-crystallization of PET-1: (1) 115 °C; (2) 117 °C; (3) 119 °C; (4) 122 °C; (5) 124 °C; (6) 126 °C.

where β is the heating rate, n is the Ozawa exponent, which depends on the dimension of crystal growth, and k is the rate constant, which is related to the overall crystallization rate and indicates how fast crystallization occurs. The above equation can be written as:

$$\ln[-\ln(1-a)] = \ln k(T) - n\ln\beta \tag{14}$$

If the above equation correctly describes the kinetics of non-isothermal crystallization, plots of $\ln[-\ln(1-\alpha)]$ versus $\ln\beta$ should give straight lines and parameters $k(T)$ and n should be obtainable from the intercepts and slopes of the lines, respectively. For PET/MWCNTs nanocomposites (PET-0.25 and PET-1) the Ozawa plots of $\ln[-\ln(1-\alpha)]$ versus $\ln\beta$ are shown in Figs. 7 and 8.

Table 3
The calculated mE_{cc} and m values of all the studied materials.

Rate	PET-0		PET-0.25		PET-0.5		PET-1		PET-2	
	mE_{cc}	m	mE_{cc}	m	mE_{cc}	m	mE_{cc}	m	mE_{cc}	m
15	427.7	4.0	322.5	2.4	442.5	2.9	402.5	2.8	409.0	2.9
10	402.8	3.7	350.7	2.6	353.7	2.3	292.8	2.1	444.0	3.2
5	469.4	4.4	393.2	2.9	401.2	2.6	365.3	2.6	446.6	3.2
2.5	515.3	4.8	371.6	2.7	358.2	2.4	319.4	2.2	494.3	3.5

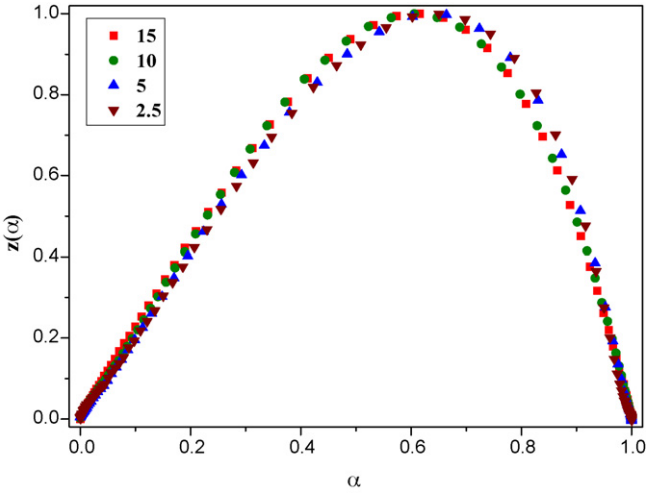

Fig. 9. Normalized $z(\alpha)$ function obtained by transformation of DSC data (for different heating rates) for the cold-crystallization of PET-0.25.

As it can be seen in these figures, straight lines are obtained for PET-0.25 at least for three different heating rates while for the PET-1 the lines are not parallel to each other. The results from the other samples are more or less analogous to PET-1. This indicates the failure of the Ozawa model to provide an adequate description of crystallization in both PET and some of its nanocomposites. Plots of $\ln[-\ln(1-\alpha)]$ versus $\ln\beta$ may be closer to linearity for some polymers when two selected temperatures are near each other or the difference of the heating rates is limited. In a more practical way since Ozawa equation ignored secondary crystallization, the reason that the non-isothermal crystallization of PET does not follow the Ozawa equation can be explained by that, at a given temperature, the crystallization processes at different heating rates are at different stages, that is, the lower heating rate process is toward the end of the crystallization process, whereas at the higher heating rate, the crystallization process is at an early stage.

The slope of the plots $\ln[-\ln(1-\alpha)]$ versus $\ln\beta$, gives directly the n-factor. It is important to note that using values that correspond to a degree of conversion in the range between 8 and 75%, for PET-0.25 and for three of the heating rates, the calculated values for the n are in the range from 2.1 to 2.4. For the other stoichiometrices since there are not linear plots corresponding to the heating rates, the n factor has not been calculated.

The dependence of the activation energy on the degree of conversion, the Avrami and Ozawa plots, give indications that for the kinetic description of the cold-crystallization of PET/MWCNTs cannot be used only one crystallization mechanism which obeys to Avrami equation. Only for the PET-0.25, one crystallization mechanism can be used, at least, for the major part of the crystallization conversion.

In order to increase the certainty regarding the applicability of the JMA model, assuming one crystallization mechanism, that arises from the above discussion, we used the second mentioned test method introduced by Malek [31] and calculated the peak position of the $z(\alpha)$ function for the different heating rates. As can be seen in Fig. 9 the peak position of the $z(\alpha)$ function, for the different heating rates, regarding to PET-0.25, stays almost constant with heating rate, $0.62 < \alpha_p < 0.65$. These values are in the acceptable range of values and we can conclude that the conditions of validity of the JMA model are satisfied for this stoichiometry and that the process is a single-step reaction. The range of α_p values of the other samples, are slightly different, with lower or larger values, from the acceptable range of values (0.62–0.64). Therefore, we can conclude that the conditions of validity of the JMA model – considering a single-step reaction – are not fully satisfied. This conclusion in accordance with the conclusion of the linearity of the Avrami and Ozawa plots for neat PET and its nanocomposites, show that in order to describe their crystallization mechanisms must be used, at least, two mechanisms with different activation energies.

These two mechanisms are, maybe, taking part in different degree of crystallization conversions for every nanocomposite. One of these is referred to the major part of the crystallization. If this part is big enough we can consider the reaction as single-step reaction as it happens for example for PET-0.25. However, their study using more than one different mechanism is a mathematical and physical complicated problem and is out of the scope of the present paper.

4.3. Conclusions

Multi-walled carbon nanotubes can act as multifunctional agents producing branched and crosslinked macromolecules by in situ polymerization of PET, when they are added at high concentrations (2 wt%). This behaviour has also affected the thermal properties of PET.

The values of the activation energy of the nanocomposites, as calculated with the OFW method, are larger than the ones of pristine PET. The activation energy presents a good stability, in the region of $0.2 < \alpha < 0.8$, and the maximum value of E in this area corresponds to PET-1. The same trend present the values of the activation energy calculated with Kissinger's method and the lower one is 107.9 kJ/mol for PET-0 while the larger is 154.0 kJ/mol for PET-1. Avrami plots have a linear portion, almost parallel to each other, which is followed by a deviation at larger temperatures; the linear portions correspond to a wide temperature and crystallization conversion range ($0.05 < \alpha < 0.80$). For neat PET this area is narrower. The calculated values of m are decreased due to the addition of MWCNTs into pristine PET. Straight lines are obtained from Ozawa plots for PET-0.25 at least for three different heating rates while for the PET-1 the lines are not parallel among them. The results from the other samples are more or less analogous to PET-1. This indicates the failure of the Ozawa model to provide an adequate description of crystallization in both PET and some of its nanocomposites. For PET-0.25 and for three of the heating rates, the calculated values for the n are in the range from 2.1 to 2.4. The dependence of the activation energy on the degree of conversion, the Avrami and Ozawa plots, give indications that for the kinetic description of the cold-crystallization of PET/MWCNTs cannot be used only one crystallization mechanism which obeys to Avrami equation. Only for PET-0.25 one crystallization mechanism can be used at least for the major part of the crystallization conversion. Malek's method showed that the conditions of validity of the JMA model are satisfied for PET-0.25 and that the process is a single-step reaction. The range of α_p values of the other samples, are slightly different, with lower or larger values, from the acceptable range of values (0.62–0.64), and thus we can conclude that the conditions of validity of the JMA model, considering a single-step reaction, are not fully fulfilled.

References

[1] M. Wu, L.L. Shaw, Int. J. Hydrogen Energy 30 (2005) 373–380.
[2] M. Wu, L.L. Shaw, J. Power Sources 136 (2004) 37–44.
[3] K. Parikh, K. Cattanach, R. Rao, D.S. Suh, A. Wu, S.K. Manohar, Sens. Actuators B 113 (2006) 55–63.
[4] Z. Li, G. Luo, F. Wei, Y. Huang, Comput. Sci. Technol. 66 (2006) 1022–1029.
[5] H.J. Lee, S.J. Oh, J.Y. Choi, J.W. Kim, J. Han, L.S. Tan, J.B. Baek, Chem. Mater. 17 (2005) 5057–5064.
[6] D.H. Shin, K.H. Yoon, O.H. Kwon, B.G. Min, C.I. Hwang, J. Appl. Polym. Sci. 99 (2006) 900–904.
[7] B.P. Grady, F. Pompeo, R.L. Shambaugh, D.E. Resasco, J. Phys. Chem. B 106 (2002) 5852.
[8] E.M. Moore, D.L. Ortiz, V.T. Marla, R.L. Shambaugh, B.P. Grady, J. Appl. Polym. Sci. 93 (2004) 2926.

[9] M.K. Seo, S.J. Park, Macromol. Mater. Eng. 289 (2004) 368.
[10] X. Zhang, T. Liu, T.V. Sreekumar, S. Kumar, V.C. Moore, R.T. Hauge, et al., Nano Lett. 3 (2003) 1285.
[11] O. Probst, E.M. Moore, D.E. Resasco, B.P. Grady, Polymer 45 (2004) 4437.
[12] T. Liu, I.Y. Phang, L. Shen, S.Y. Chow, W.-D. Zhang, Macromolecules 37 (2004) 7214.
[13] J. Li, Z. Fang, L. Tong, A. Gu, F. Liu, Eur. Polym. J. 42 (2006) 3230.
[14] D.M. Lincoln, R.A. Vaia, R. Krishnamoorti, Macromolecules 37 (2004) 4554.
[15] T.D. Fornes, D.R. Paul, Polymer 44 (2003) 3945.
[16] B.X. Fu, L. Yang, R.H. Somani, S.X. Zong, B.S. Hsiao, S. Phillips, et al., J. Polym. Sci. B: Polym. Phys. 39 (2001) 2727.
[17] A. Joshi, B.S. Butola, Polymer 45 (2004) 4953.
[18] M. Ito, K. Mizuochi, T. Kanamoto, Polymer 39 (1998) 4953.
[19] Y. Gao, Y. Wang, J. Shi, H. Bai, B. Song, Polym. Test. 27 (2008) 179.
[20] S. Tzavalas, D.E. Mouzakis, V. Drakonakis, V.G. Gregoriou, J. Polym. Sci. B: Polym. Phys. 46 (2008) 668.
[21] H.J. Yoo, Y.C. Jung, J.W. Cho, J. Polym. Sci. 46 (2008) 900.
[22] K. Chrissafis, M.I. Maragakis, K.G. Efthimiadis, E.K. Polychroniadis, J. Alloys Compd. 386 (2005) 165.
[23] M. Avrami, J. Chem. Phys. 8 (1940) 212.
[24] M. Avrami, J. Chem. Phys. 9 (1941) 177.
[25] B. Wunderlich, Macromolecular Physics, vol. 2, Academic Press, New York, 1976, p. 147.
[26] D.W. Henderson, J. Therm. Anal. 15 (1979) 325.
[27] D.W. Henderson, J. Non-Cryst. Solids 30 (1979) 301.
[28] K. Matusita, T. Konatsu, R. Yokota, J. Mater. Sci. 19 (1984) 291.
[29] J. Malek, Thermochim. Acta 138 (1989) 337.
[30] J. Malek, Thermochim. Acta 267 (1995) 61.
[31] J. Malek, Thermochim. Acta 355 (2000) 239.
[32] K. Chrissafis, Th. Kyratsi, K.M. Paraskevopoulos, M.G. Kanatzidis, Chem. Mater. 16 (2004) 1932.
[33] D.S. Achilias, D.N. Bikiaris, V. Karavelidis, G.P. Karayannidis, Eur. Polym. J. 44 (2008) 3096–3107.
[34] D. Bikiaris, V. Karavelidis, G. Karayannidis, Macromol. Rapid Commun. 27 (2006) 1199–1205.
[35] B.H. Zimm, R.W. Kilb, J. Polym. Sci. 37 (1959) 19–23.
[36] D.N. Bikiaris, G.P. Karayannidis, Polym. Int. 52 (2003) 1230–1239.
[37] G.Antoniadis, K.M. Paraskevopoulos, D. Bikiaris, K. Chrissafis, accepted for publication.
[38] I. Okazaki, B. Wunderlich, Macromolecules 30 (1997) 1758.
[39] Y. Kong, J.N. Hay, Polymer 44 (2003) 623.
[40] X.F. Lu, J.N. Hay, Polymer 42 (2001) 9423.
[41] I.A.M. Al Raheil, Polym. Int. 35 (1994) 189.
[42] B.B. Sauer, W.G. Kampert, B.E. Neal, S.A. Threefoot, B.S. Hsiao, Polymer 41 (2000) 1099.
[43] F.J. Medellin-Rodriguez, P.J. Phillips, J.S. Lin, R. Campos, J. Polym. Sci. B: Polym. Phys. 35 (1997) 1757.
[44] F.J. Medellin-Rodriguez, P.J. Phillips, J.S. Lin, Macromolecules 29 (1996) 7491.
[45] G. Karayannidis, I. Sideridou, D. Zamboulis, G. Stalidis, D. Bikiaris, N. Lazaridis, A. Wilmes, Angew. Macromol. Chem. 192 (1991) 155.
[46] K. Chrissafis, K.M. Paraskevopoulos, G.Z. Papageorgiou, D.N. Bikiaris, J. Appl. Polym. Sci. 110 (2008) 1739.
[47] J. Yang, Y. Lin, J. Wang, M. Lai, J. Li, J. Liu, X. Tong, H. Cheng, J. Appl. Polym. Sci. 98 (2005) 1087.
[48] W.J. Wang, Rubber Chem. Technol. 71 (1998) 520.
[49] D.N. Bikiaris, G.P. Karayannidis, Polym. Int. 52 (2003) 1230.
[50] G.Z. Papareorgiou, D.S. Achilias, D.N. Bikiaris, G.P. Krayannidis, J. Therm. Anal. Cal. 84 (2006) 85.
[51] Y.C. Ke, T.B. Wu, Y.F. Xia, Polymer 48 (2007) 3324–3336.
[52] G.Z. Papageorgiou, D.N. Bikiaris, D.S. Achilias, Thermochim. Acta 457 (2007) 41.
[53] S. Tzavalas, V. Drakonakis, D.E. Mouzakis, D. Fisher, V.G. Gregoriou, Macromolecules 39 (2006) 9150.
[54] K. Chrissafis, J. Therm. Anal. Cal. 95 (2009) 273.
[55] H.E. Kissinger, Anal. Chem. 29 (1957) 1702.
[56] H.E. Kissinger, J. Res. Natl. Bur. Stand. 57 (1956) 217.
[57] T. Ozawa, Bull. Chem. Soc. Jpn. 38 (1965) 1881.
[58] T. Ozawa, J. Therm. Anal. 2 (1970) 301.
[59] T. Ozawa, Polymer 12 (1971) 150.
[60] S. Vyazovkin, I. Dranca, Macromol. Chem. Phys. 207 (2006) 20.
[61] S. Vyazovkin, J. Comput. Chem. 22 (2001) 178.